SIAM J. NUMER. ANAL.
Vol. 52, No. 5, pp. 2335–2355

ON THE FULL AND GLOBAL ACCURACY OF A COMPACT THIRD ORDER WENO SCHEME*

OLIVER KOLB†

Abstract. Recently, Aràndiga et al. showed in [*SIAM J. Numer. Anal.*, 49 (2011), pp. 893–915] for a class of weighted ENO (WENO) schemes that the parameter ε occurring in the smoothness indicators of the scheme should be chosen proportional to the square of the mesh size, h^2, to achieve the optimal order of accuracy. Unfortunately, these results cannot be applied to the compact third order WENO reconstruction procedure introduced in [D. Levy, G. Puppo, and G. Russo, *SIAM J. Sci. Comput.*, 22 (2000), pp. 656–672], which we apply within the semidiscrete central scheme of [A. Kurganov and D. Levy, *SIAM J. Sci. Comput.*, 22 (2000), pp. 1461–1488], a commonly used scheme for the numerical solution of conservation laws and convection-diffusion equations. The aim of this paper is to close this gap. In particular, we will show that we achieve the optimal order of accuracy in the WENO reconstruction (h^3 in the smooth case and h^2 near discontinuities) for $\varepsilon = Kh^q$ with $q \leq 3$ and $pq \geq 2$, where $p \geq 1$ is the exponent used in the computation of the weights in the WENO scheme. Numerical examples showing the predicted order of convergence of the analyzed WENO reconstruction procedure are given as well as results for the presented semidiscrete scheme combined with a third order TVD–Runge–Kutta scheme from [S. Gottlieb and C.-W. Shu, *Math. Comp.*, 67 (1998), pp. 73–85] for the time integration.

Key words. weighted essentially nonoscillatory schemes, conservation laws, accuracy analysis, order reduction

AMS subject classifications. 65M08, 65M12

DOI. 10.1137/130947568

1. Introduction.

We consider the numerical solution of hyperbolic conservation laws

$$\frac{\partial}{\partial t}u(x,t) + \frac{\partial}{\partial x}f(u(x,t)) = 0 \tag{1.1}$$

with given initial conditions $u(x,0) = u_0(x)$. It is well known that solutions of (the weak form of) (1.1) may contain discontinuities after finite time even for arbitrary smooth initial data. Therefore, it is the challenge to achieve high resolution in regions where the solution is smooth as well as in regions where discontinuities occur or develop. While high order discretizations (without any limiting procedures) are able to efficiently resolve complex smooth solution structures, they fail in the presence of discontinuities and result in approximations with spurious oscillations.

In 1987, Harten et al. published their pioneering work on essentially nonoscillatory (ENO) schemes [11]. For the underlying piecewise polynomial reconstruction, their key idea was to choose the smoothest stencil from possible candidates. This way, high order accuracy is achieved in regions where the solution is smooth, and only slight oscillations may be produced in the presence of discontinuities, but their magnitude rapidly decreases when the grid is refined. In weighted ENO (WENO) schemes, introduced in [17], one does not choose a single stencil for the polynomial reconstruction but a convex combination of the candidate stencils, where the weighting is based on smoothness indicators. Like ENO schemes, WENO schemes are able

*Received by the editors December 4, 2013; accepted for publication (in revised form) July 24, 2014; published electronically September 25, 2014.
http://www.siam.org/journals/sinum/52-5/94756.html
†Department of Mathematics, University of Mannheim, 68131 Mannheim, Germany (kolb@uni-mannheim.de).

to resolve complex solutions with a high order of accuracy and at the same time are stable in the presence of discontinuities. The fulfillment of these two properties and in particular the respective convergence rates strongly depend on the applied smoothness indicators and the final weight design within the WENO scheme.

In the original WENO paper [17], the order of accuracy was improved by one compared to ENO schemes. Later in [13], a different smoothness indicator was proposed to obtain a fifth order WENO reconstruction from a third order ENO method. Based on the same smoothness indicators, $(2r-1)$th order WENO reconstructions (for $4 \leq r \leq 9$) were built from rth order ENO reconstructions in [2, 8].

As noted in [12] with reference to [13], WENO reconstructions may not attain the optimal order $2r-1$ at critical points, and the authors propose a fix for that problem (mapped WENO weights), which is also used in [8]. Further solution approaches to achieve the optimal order of accuracy at critical points, using a different weight design, have been considered in [18] (weighted power ENO), [4] (combination of mapped WENO and weighted power ENO), [3, 5] (WENO-Z), [22, 23] (ESWENO), [7] (improvement for mapped WENO), and recently [10].

Within the weight design of WENO schemes, a certain positive parameter (usually denoted by ε) is necessary to avoid division by zero whenever one of the smoothness indicators equals zero. Also in [12], the role of this parameter and its relation to the loss of accuracy is considered. Referring to this observation, Aràndiga et al. propose in [1] to choose the parameter ε proportional to the square of the mesh size, h^2, and they show for a class of WENO schemes (for arbitrary $r \geq 2$) that they achieve the optimal order $2r-1$ in smooth regions (also at critical points) and rth order accuracy for the presented reconstruction procedure if at least one stencil is within a smooth region. Similar results were later shown in [6], also regarding WENO-Z schemes.

Certainly, the applicability of the WENO approach goes beyond the approximate solution of (1.1) (cf. [19]). In particular, similar challenges (smooth and discontinuous solution parts/steep gradients) may occur for conservation laws with source terms or convection-diffusion equations. One very popular method for the latter problem is the third order semidiscrete central scheme introduced in [14] combined with the compact third order WENO (CTO-WENO) reconstruction from [16], e.g., together with a third order TVD Runge–Kutta scheme [9] for the time integration. In contrast with the WENO reconstruction procedure analyzed in [1], the reconstruction procedure in [16] does not only consider the reconstruction of a single point value but considers a complete quadratic polynomial in each interval of the computational grid. Further, in contrast with the original ENO or WENO approach, polynomials of different degrees are combined in the CTO-WENO reconstruction procedure. The reconstruction of complete polynomials is necessary, since in the applied semidiscrete central scheme one needs evaluations at both ends of each grid interval and moreover further evaluations (e.g., approximate derivatives) are required when solving, for instance, convection-diffusion equations (cf. [14]). Unfortunately, as a consequence of the noted differences, the results of [1] cannot be applied directly to the CTO-WENO scheme resulting from [14, 16], and it is the aim of this paper to close this gap.

For the approximate solution of (1.1), we apply the semidiscrete central scheme from [14] with the CTO-WENO reconstruction procedure of [16] and a third order TVD Runge–Kutta scheme [9]. According to the results in [1], we choose the parameter ε, which occurs in the computation of the weights in the reconstruction procedure, dependent on the mesh size h, namely, $\varepsilon = \varepsilon(h) = Kh^q$. The main issue will be the

analysis of the convergence properties of the resulting CTO-WENO reconstruction. As will be shown below, the admissible range for the exponent q in $\varepsilon(h)$ to achieve the optimal order (here h^3 in the smooth case and h^2 near discontinuities) is larger than in [1]. We need $q \leq 3$ and $pq \geq 2$, where $p \geq 1$ is another parameter, the exponent used in the computation of the weights in the CTO-WENO scheme. Thus, for the usual choice $p = 2$, we get the optimal order in the reconstruction step for $q \in [1, 3]$.

The outline of this paper is as follows. The entire scheme including our main results is described in section 2. In section 3 we prove that the presented scheme fulfills the assumptions made within our main results. We give some numerical evidence of the performed analysis in section 4 and our conclusions in section 5.

2. Numerical scheme. The main ingredient of the analyzed scheme to numerically solve (1.1) is the underlying CTO-WENO reconstruction procedure based on cell averages, which is described in section 2.1. Afterward, we present our main results in section 2.2 and the fully discrete scheme to approximately solve (1.1) in section 2.3.

2.1. Reconstruction procedure. We give a brief description of the applied CTO-WENO reconstruction procedure, mainly following [16]. Since this procedure is independent of the time variable, we consider $u = u(x)$ as function of the spatial variable only. Further, we assume a uniform grid with spatial grid size h, grid points $x_j = x_0 + jh$, and corresponding finite volumes $I_j = [x_j - \frac{h}{2}, x_j + \frac{h}{2}] = [x_{j-\frac{1}{2}}, x_{j+\frac{1}{2}}]$. Based on cell averages $\bar{u}_j$ over all I_j,

$$\bar{u}_j = \frac{1}{h} \int_{x_{j-\frac{1}{2}}}^{x_{j+\frac{1}{2}}} u(x)\, dx,$$

the aim is to reconstruct the underlying function u by a piecewise polynomial approximation P. For this, we will use (in each cell I_j) a convex combination of three polynomials P_{L}, P_{C}, and P_{R},

$$P(x) = w_{\mathrm{L}} P_{\mathrm{L}}(x) + w_{\mathrm{C}} P_{\mathrm{C}}(x) + w_{\mathrm{R}} P_{\mathrm{R}}(x) \tag{2.1}$$

with $w_i \geq 0$ for all $i \in \{\mathrm{L}, \mathrm{C}, \mathrm{R}\}$ and $w_{\mathrm{L}} + w_{\mathrm{C}} + w_{\mathrm{R}} = 1$. Here and also later, to improve the readability, we leave out the index j, indicating the considered interval for the polynomials and other terms, wherever it is clear from the context.

The polynomials P_{L} and P_{R} are one-sided linear reconstructions, uniquely determined by imposing the conservation of the cell averages $\bar{u}_{j-1}$ over I_{j-1} and $\bar{u}_j$ over I_j for P_{L}, and $\bar{u}_j$ over I_j and $\bar{u}_{j+1}$ over I_{j+1} for P_{R}, resulting in

$$P_{\mathrm{L}}(x) = \bar{u}_j + \frac{\bar{u}_j - \bar{u}_{j-1}}{h}(x - x_j), \qquad P_{\mathrm{R}}(x) = \bar{u}_j + \frac{\bar{u}_{j+1} - \bar{u}_j}{h}(x - x_j).$$

The third polynomial P_{C} is a parabola, chosen in such a way that

$$P_{\mathrm{opt}}(x) = c_{\mathrm{L}} P_{\mathrm{L}}(x) + c_{\mathrm{C}} P_{\mathrm{C}}(x) + c_{\mathrm{R}} P_{\mathrm{R}}(x) \tag{2.2}$$

with constants c_{L}, c_{R}, and $c_{\mathrm{C}} = 1 - c_{\mathrm{L}} - c_{\mathrm{R}}$, where P_{opt} is the unique parabola conserving the three cell averages $\bar{u}_{j-1}$, $\bar{u}_j$, $\bar{u}_{j+1}$ over I_{j-1}, I_j and I_{j+1}, i.e.,

$$\frac{1}{h} \int_{x_{j-\frac{1}{2}+l}}^{x_{j+\frac{1}{2}+l}} P_{\mathrm{opt}}(x)\, dx = \bar{u}_{j+l} \qquad \forall l \in \{-1, 0, 1\}.$$

The latter conditions yield

$$P_{\text{opt}}(x) = u_j + u_j'(x - x_j) + \frac{1}{2}u_j''(x - x_j)^2$$

with

$$u_j = \bar{u}_j - \frac{1}{24}\big(\bar{u}_{j+1} - 2\bar{u}_j + \bar{u}_{j-1}\big),$$
$$u_j' = \frac{\bar{u}_{j+1} - \bar{u}_{j-1}}{2h}, \quad u_j'' = \frac{\bar{u}_{j+1} - 2\bar{u}_j + \bar{u}_{j-1}}{h^2}.$$

For sufficiently smooth u (e.g., $u \in C^3(\mathbb{R})$), choosing the "optimal" polynomials P_{opt} in each interval I_j locally results in a third order reconstruction, i.e.,

$$P(x) = P_{\text{opt}}(x) = u(x) + \mathcal{O}(h^3) \qquad \forall x \in I_j.$$

However, in the case of discontinuities, the application of $P = P_{\text{opt}}$ in each interval would result in an oscillatory reconstruction. For this reason, we apply (2.1) with

$$w_i = \frac{\alpha_i}{\sum_k \alpha_k}, \quad \text{where} \quad \alpha_i = \frac{c_i}{(\varepsilon(h) + IS_i)^p}, \quad i, k \in \{\text{L}, \text{C}, \text{R}\}, \tag{2.3}$$

and the smoothness indicators

$$IS_i = \sum_{k=1}^{2} \int_{x_{j-\frac{1}{2}}}^{x_{j+\frac{1}{2}}} h^{2k-1}\big(P_i^{(k)}(x)\big)^2 dx, \qquad i \in \{\text{L}, \text{C}, \text{R}\}.$$

For the polynomials P_{L}, P_{C}, P_{R} above, when choosing $c_{\text{L}} = c_{\text{R}}$, this yields

$$IS_{\text{L}} = (\bar{u}_j - \bar{u}_{j-1})^2, \qquad IS_{\text{R}} = (\bar{u}_{j+1} - \bar{u}_j)^2,$$
$$IS_{\text{C}} = \frac{13}{12c_{\text{C}}^2}(\bar{u}_{j+1} - 2\bar{u}_j + \bar{u}_{j-1})^2 + \frac{1}{4}(\bar{u}_{j+1} - \bar{u}_{j-1})^2. \tag{2.4}$$

Usually, $p = 2$ is used in (2.3) and also a constant value for the parameter $\varepsilon(h)$, originally introduced to avoid division by zero or very small numbers. As already considered in [1, 12], the latter parameter plays a crucial role for the accuracy and the stability of the entire scheme. Therefore, we use $\varepsilon(h) = Kh^q$ dependent on the mesh size h (cf. [1], where $q = 2$). For the constants c_i in (2.2) and (2.3), we use $c_{\text{L}} = c_{\text{R}} = 0.25$ as in [16] and accordingly $c_{\text{C}} = 1 - c_{\text{L}} - c_{\text{R}} = 0.5$. Note that a symmetric choice for these constants is essential to get third order accuracy when the presented CTO-WENO reconstruction is used in combination with staggered grids.

For later use, since the polynomials P_{L}, P_{C}, and P_{R} are affected by u from different regions, we introduce the following stencils/regions of dependence:

$$S_{\text{L}} = I_{j-1} \cup I_j, \qquad S_{\text{C}} = I_{j-1} \cup I_j \cup I_{j+1}, \qquad S_{\text{R}} = I_j \cup I_{j+1}.$$

Remark 2.1. The presented CTO-WENO reconstruction procedure (and also the fully discrete scheme described in section 2.3) can as well be applied for vector-valued u, corresponding to the case of a system of conservation laws. For this, the reconstruction can be performed componentwise or using combined smoothness indicators (cf. [15]).

2.2. Main results. We will now formulate the main results of this work. In section 3 below, we will show under which conditions the weights w_i fulfill the assumptions made in Theorems 2.1 and 2.2.

First, we show that the presented CTO-WENO reconstruction procedure is third order accurate in the smooth case.

THEOREM 2.1. *We assume that in smooth regions*

$$w_i = c_i + \mathcal{O}(h^r) \qquad \forall i \in \{_L, _C, _R\}$$

holds with $r \geq 1$. Then, if u is smooth in the stencil S_C, we have

$$u(x) - P(x) = \mathcal{O}(h^3) \tag{2.5}$$

for all $x \in I_j$, where P is given by (2.1) *and the weights and polynomials are as described in section* 2.1.

Proof. We consider

$$u(x) - P(x) = u(x) - P_{\text{opt}}(x) + P_{\text{opt}}(x) - P(x).$$

From the theory of polynomial interpolation, we know that

$$u(x) - P_{\text{opt}}(x) = \mathcal{O}(h^3)$$

for smooth u. Thus, it remains to show that

$$P_{\text{opt}}(x) - P(x) = \mathcal{O}(h^3). \tag{2.6}$$

Since $c_{\text{L}} + c_{\text{C}} + c_{\text{R}} = 1 = w_{\text{L}} + w_{\text{C}} + w_{\text{R}}$, we get

$$\begin{aligned} P_{\text{opt}}(x) - P(x) &= \sum_i c_i P_i(x) - \sum_i w_i P_i(x) \\ &= \sum_i (c_i - w_i)\, P_i(x) = \sum_i (c_i - w_i)\big(P_i(x) - u(x)\big). \end{aligned}$$

Again from the theory of polynomial interpolation, we know that

$$P_i(x) - u(x) = \mathcal{O}(h^2)$$

at least. Along with the assumption that $c_i - w_i = \mathcal{O}(h^r)$ with $r \geq 1$, we finally get (2.6) and therewith (2.5). ∎

Next, we consider the nonsmooth case. Note that if the stencil S_{L} or S_{R} contains a discontinuity, then it is also contained in S_{C}.

THEOREM 2.2. *Let u be smooth in one of the stencils S_L or S_R and let the other stencil contain a discontinuity. If the weights satisfy*

$$w_i = \begin{cases} \mathcal{O}(1) & \text{if } u \text{ is smooth in } S_i, \\ \mathcal{O}(h^{\tilde{r}}) & \text{if } u \text{ has a discontinuity in } S_i, \end{cases} \tag{2.7}$$

with $\tilde{r} \geq 2$, then

$$u(x) - P(x) = \mathcal{O}(h^2) \tag{2.8}$$

for all $x \in I_j$, where P is given by (2.1) *and the weights and polynomials are as described in section* 2.1.

Proof. Since $w_{\mathrm{L}} + w_{\mathrm{C}} + w_{\mathrm{R}} = 1$, we have

$$u(x) - P(x) = \sum_i w_i \big(u(x) - P_i(x)\big). \tag{2.9}$$

Now let $D \subset \{\mathrm{L}, \mathrm{C}, \mathrm{R}\}$ be the indices of the (two) stencils S_i which contain the discontinuity. Then we get from (2.9)

$$u(x) - P(x) = \sum_{i \in D} \underbrace{w_i}_{=\mathcal{O}(h^{\tilde r})} \underbrace{\big(u(x) - P_i(x)\big)}_{=\mathcal{O}(1)} + \sum_{i \notin D} \underbrace{w_i}_{=\mathcal{O}(1)} \underbrace{\big(u(x) - P_i(x)\big)}_{\mathcal{O}(h^2)} = \mathcal{O}(h^2) \tag{2.10}$$

since $\tilde r \geq 2$. The $\mathcal{O}(1)$ term for the interpolation error in the discontinuous case directly results from the construction of the polynomials P_i as a worst-case estimate since $x - x_j = \mathcal{O}(h)$. ∎

2.3. Fully discrete scheme. Since it is used in the numerical examples below, we give a brief description of a complete numerical scheme to solve (1.1) based on the CTO-WENO reconstruction procedure presented in section 2.1 (cf. [14]). As noted in Remark 2.1, the whole scheme can also be applied to systems of conservation laws. For this, we apply the reconstruction procedure componentwise.

For a given mesh size h, the first step toward solving (1.1) consists of averaging over all intervals I_j. In particular, we get the initial cell averages

$$\bar u_j(0) = \frac{1}{h} \int_{x_{j-\frac12}}^{x_{j+\frac12}} u_0(x)\,dx, \tag{2.11}$$

and for the evolution of the cell averages in each interval I_j

$$\frac{\partial}{\partial t} \bar u_j(t) = -\frac{1}{h} \big(f(u(x_{j+\frac12}, t)) - f(u(x_{j-\frac12}, t))\big).$$

Next, the fluxes $f(u(x_{j\pm\frac12}, t))$ at the cell boundaries are replaced/approximated by a numerical flux function $H_{j\pm\frac12}(t)$ given by

$$H_{j+\frac12}(t) = \frac{f(u^+_{j+\frac12}(t)) + f(u^-_{j+\frac12}(t))}{2} - \frac{a_{j+\frac12}(t)}{2} \big(u^+_{j+\frac12}(t) - u^-_{j+\frac12}(t)\big) \tag{2.12}$$

with

$$a_{j+\frac12}(t) = \max_{u \in C(u^-_{j+\frac12}(t), u^+_{j+\frac12}(t))} \rho\left(\frac{\partial f}{\partial u}(u)\right) \tag{2.13}$$

and

$$u^-_{j+\frac12}(t) = P_j(x_{j+\frac12}, t) \qquad \text{and} \qquad u^+_{j+\frac12}(t) = P_{j+1}(x_{j+\frac12}, t).$$

Here, P_j and P_{j+1} are reconstructed from the cell averages at time t according to the procedure described in section 2.1. Further, $\rho(A)$ denotes the spectral radius of the matrix A and $C(u^-_{j+\frac12}(t), u^+_{j+\frac12}(t))$ is the curve in the phase space that connects $u^-_{j+\frac12}(t)$ and $u^+_{j+\frac12}(t)$ via a Riemann fan. Note that (2.13) can be easily evaluated in the genuinely nonlinear or linearly degenerate case, where it reduces to

$$a_{j+\frac12}(t) = \max\left\{ \rho\left(\frac{\partial f}{\partial u}\big(u^-_{j+\frac12}(t)\big)\right), \rho\left(\frac{\partial f}{\partial u}\big(u^+_{j+\frac12}(t)\big)\right)\right\}.$$

Furthermore note that the numerical flux function in (2.12) corresponds to a local Lax–Friedrichs flux. Finally, the third order TVD Runge–Kutta scheme of [9] is used for the time integration of the semidiscretized problem

$$\frac{\partial}{\partial t}\bar{u}_j(t) = -\frac{1}{h}\big(H_{j+\frac{1}{2}}(t) - H_{j-\frac{1}{2}}(t)\big)$$

with initial conditions (2.11).

3. Accuracy analysis. The aim of this section is to prove the properties of the smoothness indicators and the resulting weights, which are necessary for the convergence results given in Theorems 2.1 and 2.2.

3.1. The smoothness indicators. For given grid points x_j we define

$$s_j = \begin{cases} 0 & \text{if } u'(x_j) \neq 0, \\ \max\left\{k \in \mathbb{N} :\ u^{(i)}(x_j) = 0,\ 1 \le i \le k\right\} & \text{otherwise,} \end{cases}$$

where we assume $s_j < \infty$.

LEMMA 3.1. *Whenever u is smooth enough in the respective stencil, then the smoothness indicators* (2.4) *may be written as*

$$\begin{aligned} IS_L &= \bar{a}_j h^{2s_j+2} - \bar{b}_j h^{2s_j+3} + \mathcal{O}(h^{2s_j+4}), \\ IS_C &= \bar{a}_j h^{2s_j+2} \cdot \begin{cases} 1 & \textit{if } s_j \textit{ is even} \\ \dfrac{13}{3c_C^2} & \textit{if } s_j \textit{ is odd} \end{cases} + \mathcal{O}(h^{2s_j+4}), \\ IS_R &= \bar{a}_j h^{2s_j+2} + \bar{b}_j h^{2s_j+3} + \mathcal{O}(h^{2s_j+4}) \end{aligned}$$

with constants $\bar{a}_j > 0$, $\bar{b}_j \in \mathbb{R}$ being dependent only on the position x_j but not on the discretization parameter h.

Proof. Throughout the proof we will leave out the index j in s_j and further constants to improve the readability. For u sufficiently smooth, Taylor expansion gives

$$\begin{aligned} u(x_j + d) = u(x_j) &+ \frac{d^{s+1}}{(s+1)!}u^{(s+1)}(x_j) + \frac{d^{s+2}}{(s+2)!}u^{(s+2)}(x_j) \\ &+ \frac{d^{s+3}}{(s+3)!}u^{(s+3)}(x_j) + \mathcal{O}(d^{s+4}) \end{aligned} \tag{3.1}$$

and for $2 \le k \le s+2$

$$\begin{aligned} u^{(k-1)}(x_j + d) = \frac{d^{s+2-k}}{(s+2-k)!}u^{(s+1)}(x_j) &+ \frac{d^{s+3-k}}{(s+3-k)!}u^{(s+2)}(x_j) \\ &+ \frac{d^{s+4-k}}{(s+4-k)!}u^{(s+3)}(x_j) + \mathcal{O}(d^{s+5-k}). \end{aligned} \tag{3.2}$$

Now, let U be a primitive of u; then

$$\bar{u}(x) = \frac{1}{h}\int_{x-\frac{h}{2}}^{x+\frac{h}{2}} u(y)\,dy = \frac{1}{h}\left(U\left(x + \frac{h}{2}\right) - U\left(x - \frac{h}{2}\right)\right)$$

and assuming (enough) smoothness

$$\begin{aligned}\bar{u}^{(k)}(x) &= \frac{1}{h}\left(U^{(k)}\left(x+\frac{h}{2}\right) - U^{(k)}\left(x-\frac{h}{2}\right)\right)\\ &= \frac{1}{h}\left(u^{(k-1)}\left(x+\frac{h}{2}\right) - u^{(k-1)}\left(x-\frac{h}{2}\right)\right).\end{aligned}$$

Inserting (3.1) and (3.2) with $d = \frac{h}{2}$ gives for $x = x_j$ and $1 \le k \le s+2$

$$\bar{u}^{(k)}(x_j) = \begin{cases} \dfrac{u^{(s+2)}(x_j)}{(s+3-k)!\,2^{s+2-k}}h^{s+2-k} + \mathcal{O}(h^{s+4-k}) & \text{if } s-k \text{ is even},\\ \dfrac{u^{(s+1)}(x_j)}{(s+2-k)!\,2^{s+1-k}}h^{s+1-k} + \mathcal{O}(h^{s+3-k}) & \text{if } s-k \text{ is odd}.\end{cases} \tag{3.3}$$

Next, Taylor expansion of $\bar{u}_{j+1} = \bar{u}(x_{j+1})$ yields

$$\bar{u}_{j+1} = \bar{u}_j + \sum_{k=1}^{s+2}\frac{h^k}{k!}\bar{u}^{(k)}(x_j) + \mathcal{O}(h^{s+3}).$$

Making use of (3.3) gives

$$\bar{u}_{j+1} = \bar{u}_j + a_{s+1}h^{s+1} + a_{s+2}h^{s+2} + \mathcal{O}(h^{s+3}) \tag{3.4}$$

with

$$a_{s+1} = u^{(s+1)}(x_j)\cdot\begin{cases}\displaystyle\sum_{k=1}^{\frac{s}{2}+1}\frac{1}{(2k-1)!\,(s+3-2k)!\,2^{s+2-2k}} & \text{if } s \text{ is even},\\ \displaystyle\sum_{k=1}^{\frac{s-1}{2}+1}\frac{1}{(2k)!\,(s+2-2k)!\,2^{s+1-2k}} & \text{if } s \text{ is odd},\end{cases}$$

$$a_{s+2} = u^{(s+2)}(x_j)\cdot\begin{cases}\displaystyle\sum_{k=1}^{\frac{s}{2}+1}\frac{1}{(2k)!\,(s+3-2k)!\,2^{s+2-2k}} & \text{if } s \text{ is even},\\ \displaystyle\sum_{k=1}^{\frac{s+1}{2}+1}\frac{1}{(2k-1)!\,(s+4-2k)!\,2^{s+3-2k}} & \text{if } s \text{ is odd}.\end{cases}$$

Accordingly, Taylor expansion of $\bar{u}_{j-1}$ yields

$$\bar{u}_{j-1} = \bar{u}_j + (-1)^{s+1}a_{s+1}h^{s+1} + (-1)^{s+2}a_{s+2}h^{s+2} + \mathcal{O}(h^{s+3}). \tag{3.5}$$

We define

$$\bar{a} = (a_{s+1})^2, \qquad \bar{b} = 2a_{s+1}a_{s+2}.$$

Then, inserting (3.4) and (3.5) into the smoothness indicators (2.4) directly gives the desired form. ∎

LEMMA 3.2. *If u is sufficiently smooth in I_j and the neighboring cells, and $q \le 3$, then there exist constants e_{ik} such that*

$$\frac{IS_i - IS_k}{\varepsilon(h) + IS_k} = e_{ik}h^r + \mathcal{O}(h^{r+1}) \tag{3.6}$$

with $r \geq 1$, and

$$\frac{\varepsilon(h) + IS_i}{\varepsilon(h) + IS_k} = 1 + \mathcal{O}(h^r) \tag{3.7}$$

with the same r holds.

Proof. With Lemma 3.1 we get from the smoothness assumption that the smoothness indicators may be written in the form

$$IS_i = a_i h^{2s+2} + b_i h^{2s+3} + \mathcal{O}(h^{2s+4}) \tag{3.8}$$

and therewith

$$IS_i - IS_k = c_{ik} h^{2s+2} + d_{ik} h^{2s+3} + \mathcal{O}(h^{2s+4}) \tag{3.9}$$

holds with appropriate constants a_i and b_i, $c_{ik} = a_i - a_k$, and $d_{ik} = b_i - b_k$. Making use of (3.8) and (3.9) we have

$$\frac{IS_i - IS_k}{\varepsilon(h) + IS_k} = \frac{c_{ik} h^{2s+2} + d_{ik} h^{2s+3} + \mathcal{O}(h^{2s+4})}{K h^q + a_k h^{2s+2} + b_k h^{2s+3} + \mathcal{O}(h^{2s+4})}. \tag{3.10}$$

In the case that s is even, we see from Lemma 3.1 that $c_{ik} = 0$. Thus, dividing through by h^z with $z = \min(q, 2s+2)$ leads to the desired form with $r = 2s+3-z \geq 1$.

If s is odd and therefore $s \geq 1$, we have $2s + 2 \geq 4$, and dividing through by h^q leads to the desired form with $r = 2s + 2 - q \geq 1$ (since $q \leq 3$ by assumption).

From the previous result, we directly get

$$\frac{\varepsilon(h) + IS_i}{\varepsilon(h) + IS_k} = \frac{\varepsilon(h) + IS_k - IS_k + IS_i}{\varepsilon(h) + IS_k} = 1 + \frac{IS_i - IS_k}{\varepsilon(h) + IS_k} = 1 + \mathcal{O}(h^r). \qquad \square$$

Remark 3.1. In [16] the authors impose $\varepsilon + h^2 u_x^2 \gg |IS - h^2 u_x^2|$ in smooth regions, which corresponds to $\varepsilon(h) + IS_k \gg |IS_i - IS_k|$ in this work; more precisely, $\frac{IS_i - IS_k}{\varepsilon(h) + IS_k} = \mathcal{O}(h)$ (see (3.6)).

3.2. The weights. Based on the results in the previous section, we may show the following theorem for the weights of the presented CTO-WENO reconstruction in the smooth case.

THEOREM 3.3. *If u is sufficiently smooth in I_j and the neighboring cells, and $q \leq 3$, then*

$$w_i = c_i + \mathcal{O}(h^r) \qquad \forall i \in \{_L, _C, _R\}$$

holds with $r \geq 1$ for arbitrary $p \in \mathbb{N}$.

Proof. From the generalization of the third binomial formula, we deduce (cf. [1])

$$\frac{1}{(\varepsilon(h) + IS_k)^p} = \frac{1}{(\varepsilon(h) + IS_i)^p} \left(1 + \underbrace{\frac{IS_i - IS_k}{\varepsilon(h) + IS_k}}_{= e_{ik} h^r + \mathcal{O}(h^{r+1})} \sum_{t=0}^{p-1} \underbrace{\left(\frac{\varepsilon(h) + IS_i}{\varepsilon(h) + IS_k} \right)^t}_{= 1 + \mathcal{O}(h^r)} \right)$$

and together with the results of Lemma 3.2

$$\frac{1}{(\varepsilon(h) + IS_k)^p} = \frac{1}{(\varepsilon(h) + IS_i)^p} \left(1 + p e_{ik} h^r + \mathcal{O}(h^{r+1}) \right). \tag{3.11}$$

Computing α_k according to (2.3) yields

$$\alpha_k = \frac{c_k}{(\varepsilon(h) + IS_k)^p} \overset{(3.11)}{=} \frac{c_k}{(\varepsilon(h) + IS_i)^p} \left(1 + pe_{ik}h^r + \mathcal{O}(h^{r+1})\right)$$

and thus (for arbitrary $i \in \{\text{L}, \text{C}, \text{R}\}$)

$$\begin{aligned} \sum_k \alpha_k &= \frac{1}{(\varepsilon(h) + IS_i)^p} \sum_k c_k \left(1 + pe_{ik}h^r + \mathcal{O}(h^{r+1})\right) \\ &= \frac{1}{(\varepsilon(h) + IS_i)^p} \left(\underbrace{\sum_k c_k}_{=1} + \Big(p \underbrace{\sum_k c_k e_{ik}}_{=: -f_i} \Big) h^r + \mathcal{O}(h^{r+1}) \right) \\ &= \frac{1}{(\varepsilon(h) + IS_i)^p} \left(1 - pf_i h^r + \mathcal{O}(h^{r+1})\right). \end{aligned} \tag{3.12}$$

With (3.12) at hand, we finally get for the weights

$$w_i = \frac{\alpha_i}{\sum_k \alpha_k} = \frac{c_i}{1 - pf_i h^r + \mathcal{O}(h^{r+1})} = c_i \left(1 + pf_i h^r + \mathcal{O}(h^{r+1})\right) \tag{3.13}$$

and in particular

$$w_i = c_i + \mathcal{O}(h^r) \qquad \forall i \in \{\text{L}, \text{C}, \text{R}\}$$

with $r \geq 1$ as in Lemma 3.2. ∎

Remark 3.2. In Theorem 3.3 we showed that the weights of the presented CTO-WENO reconstruction procedure fulfill the requirements of Theorem 2.1. As can be seen from the proof of Lemma 3.2 (which is applied in the proof of Theorem 3.3), the condition $q \leq 3$ is necessary for the case $s \geq 1$, i.e., at critical points. If $s \geq 1$, $q > 3$ might lead to an order reduction, since the essential condition $r \geq 1$ cannot be satisfied. A similar behavior can be expected for the constant choice $\varepsilon(h) \approx 0$. Considering the limit case ($h \to 0$), we note that this order reduction is observed at the point x where the first derivative vanishes, whether or not x corresponds to a grid point x_j, as can be seen in the numerical results in section 4.1.

Next, we show the requirements on the weights in the nonsmooth case.

THEOREM 3.4. *Let u be smooth in one of the stencils S_L or S_R and let the other stencil contain a discontinuity. Further let $p \geq 1$ and $pq \geq 2$. Then the weights given by* (2.3) *satisfy*

$$w_i = \begin{cases} \mathcal{O}(1) & \text{if } u \text{ is smooth in } S_i, \\ \mathcal{O}(h^{\tilde{r}}) & \text{if } u \text{ has a discontinuity in } S_i \end{cases} \tag{3.14}$$

with $\tilde{r} \geq 2$.

Proof. Without loss of generality let us assume that u is smooth in S_L and there is a discontinuity in S_R and therewith also S_C (with jump Δu). In this case, we have

$$IS_\text{L} = \bar{a}h^{2s+2} + \mathcal{O}(h^{2s+3})$$

according to Lemma 3.1, and obviously neither IS_{C} nor IS_{R} converges toward zero for $h \to 0$, but both are $\Theta(\Delta u)$. Therefore, we have

$$\alpha_{\mathrm{R}} = \Theta\big(1/(\Delta u)^p\big) \qquad \text{and} \qquad \alpha_{\mathrm{C}} = \Theta\big(1/(\Delta u)^p\big), \tag{3.15}$$

and

$$\alpha_{\mathrm{L}} = \frac{c_{\mathrm{L}}}{\big(Kh^q + \bar{a}h^{2s+2} + \mathcal{O}(h^{2s+3})\big)^p} = \frac{\tilde{c}_{\mathrm{L}}}{h^{pz} + \mathcal{O}(h^{pz+\delta})} = \Theta(h^{-pz})$$

with $z = \min(q, 2s+2)$ and some $\delta > 0$. For $q > 0$ this yields

$$\sum_k \alpha_k = \Theta(h^{-pz})$$

and therewith

$$w_{\mathrm{L}} = \mathcal{O}(1), \qquad w_{\mathrm{C}} = \mathcal{O}(h^{pz}), \qquad \text{and} \qquad w_{\mathrm{R}} = \mathcal{O}(h^{pz}).$$

Due to $p \geq 1$ and $pq \geq 2$ we directly get the desired result with $\tilde{r} = pz \geq 2$. ∎

Remark 3.3. If the parameter q is chosen smaller than $2/p$, one obviously cannot prove $\tilde{r} \geq 2$, which is essential for the second order accuracy statement in Theorem 2.2. Note that a constant $\varepsilon(h)$, corresponding to $q = 0$, also falls within this case. Nevertheless, as long as the term $\varepsilon(h) = Kh^q = K$ is significantly smaller than the smoothness indicator corresponding to the stencil where u is smooth (which is $\mathcal{O}(h^{2s+2})$), a second order decrease in the computed error can be observed (see section 4.1).

Remark 3.4. In [16] the authors impose $\varepsilon \ll IS$ near discontinuities. Within this work, this condition is fulfilled for $q > 0$ (and $h \to 0$) and it is necessary for (3.15) in the proof of Theorem 3.4.

4. Numerical results. Within this section we consider several well-known problems from literature. While section 4.1 is supposed to numerically confirm the analytical results of section 2.2 for the applied CTO-WENO reconstruction procedure, sections 4.2 to 4.4 show results for the fully discrete scheme presented in section 2.3.

4.1. Reconstruction in the smooth and the discontinuous case. In the first example (adapted from [1, 12]), we consider the accuracy of the reconstruction procedure from section 2.1 for the smooth function

$$u_s(x) = x^3 + \cos(x)$$

and also

$$u_d(x) = u_s(x) + H(x)$$

with

$$H(x) = \begin{cases} 1 & \text{if } x > 0, \\ 0 & \text{else.} \end{cases}$$

The point we are particularly interested in is $x = 0$, because $u_s'(0) = 0$ and u_d has its discontinuity at $x = 0$. Therefore, we consider the reconstruction within $I_j = [-h, 0]$ (for $h = 0.8 \cdot 2^{-n}$ with $n \in \{1, \ldots, 14\}$), evaluate the resulting polynomials at $x = 0$,

and compare with $u_s(0) = 1$ and $u_d(0) = 1$. Note that $u_d(0)$ is chosen in such a way that the stencil $S_{\text{L}} = [-2h, 0]$ completely lies within a smooth region of u_d. To confirm our analytical results from section 2.2, we apply a broad choice for $\varepsilon(h)$ and p, namely, $\varepsilon(h) \in \{10^{20}, h^1, 10^{-3}, 10^{-6}, 10^{-100}\}$ and $\varepsilon(h) \in \{h^{0.5}, h^1, h^2, h^3, h^4\}$ for $p = 2$, $\varepsilon(h) \in \{h^1, h^2, h^3, h^4\}$ for $p = 1$ and $\varepsilon(h) \in \{h^{0.25}, h^{0.5}, h^3, h^4\}$ for $p = 4$.

The first set is supposed to demonstrate the difference between a constant choice for $\varepsilon(h)$ and the variable version. For $\varepsilon(h) = 10^{20}$ the contribution of the smoothness indicators in the computation of the weights according to (2.3) is negligible and thus this case corresponds to the choice of $P = P_{\text{opt}}$ as reconstruction, which should only work properly in the smooth case. Using $\varepsilon(h) = 10^{-100}$ is somehow the opposite, since here merely division by zero is avoided, but $\varepsilon(h)$ has no further significant influence on the computations. Finally, $\varepsilon(h) = 10^{-3}$ and $\varepsilon(h) = 10^{-6}$ are supposed to cover a representative range of usual choices.

The three further sets are supposed to numerically validate the bounds for the exponent q in $\varepsilon(h) = h^q$. Here, $q > 3$ should always lead to an order reduction at critical points in the smooth case (compare Remark 3.2), and each choice with $q < 2/p$ should lead to an order reduction in the discontinuous case (compare Remark 3.3).

Tables 1, 2, 3, and 4 show the reconstruction errors $|P(0)-u_s(0)|$ and the resulting convergence rates (c.r.). Here and also later, to improve the readability within the tables, we use bold characters wherever $\varepsilon(h) = h^q \leq 10^{-3}$, and we use italics for all entries with $h^q \leq 10^{-6}$. As noted above, the choice $\varepsilon(h) = 10^{20}$, which basically means $P \approx P_{\text{opt}}$, perfectly shows third order accuracy for this smooth example. Also for $\varepsilon(h) = h^1$ and $\varepsilon(h) = 10^{-3}$, the expected formal order can be directly observed, whereas for the smaller choice $\varepsilon(h) = 10^{-6}$ a finer grid resolution is necessary to achieve third order (and also the errors are larger at the beginning). This effect is a potential drawback when $\varepsilon(h)$ is chosen too small. Finally, using $\varepsilon(h) = 10^{-100} \approx 0$ results in an order reduction as already noted in Remark 3.2. The same effect occurs for $\varepsilon(h) = h^q$ with $q = 4 > 3$ in Tables 2, 3, and 4. On the other hand, third order convergence can be observed for all other choices with $q \leq 3$. Here, for the smaller exponents, which in turn means larger values for $\varepsilon(h)$, the formal order is achieved earlier. To a certain extent independent of whether the corresponding errors are actually (much) smaller, reliably reaching the expected formal convergence rate

TABLE 1
Reconstruction results for $u_s(x)$ at $x = 0$ with $p = 2$.

n	10^{20}		h^1		10^{-3}		10^{-6}		10^{-100}	
	Error	c.r.	Error	c.r.	Error	c.r.	Error	c.r.	Error	c.r.
1	3.12e-02	–	2.87e-02	–	2.64e-02	–	2.64e-02	–	2.64e-02	–
2	3.95e-03	3.0	4.17e-03	2.8	5.61e-03	2.2	6.65e-03	2.0	6.65e-03	2.0
3	4.97e-04	3.0	5.01e-04	3.1	6.04e-04	3.2	1.67e-03	2.0	1.67e-03	2.0
4	6.23e-05	3.0	6.24e-05	3.0	6.70e-05	3.2	4.01e-04	2.1	4.17e-04	2.0
5	7.80e-06	3.0	7.80e-06	3.0	7.86e-06	3.1	3.52e-06	6.8	1.04e-04	2.0
6	9.76e-07	3.0	9.76e-07	3.0	9.77e-07	3.0	1.75e-06	1.0	2.60e-05	2.0
7	1.22e-07	3.0	1.22e-07	3.0	1.22e-07	3.0	1.35e-07	3.7	6.51e-06	2.0
8	1.53e-08	3.0	1.53e-08	3.0	1.53e-08	3.0	1.55e-08	3.1	1.63e-06	2.0
9	1.91e-09	3.0	1.91e-09	3.0	1.91e-09	3.0	1.91e-09	3.0	4.07e-07	2.0
10	2.38e-10	3.0	**2.38e-10**	3.0	2.38e-10	3.0	2.38e-10	3.0	1.02e-07	2.0
11	2.98e-11	3.0	**2.98e-11**	3.0	2.98e-11	3.0	2.98e-11	3.0	2.54e-08	2.0
12	3.73e-12	3.0	**3.73e-12**	3.0	3.73e-12	3.0	3.73e-12	3.0	6.36e-09	2.0
13	4.66e-13	3.0	**4.66e-13**	3.0	4.66e-13	3.0	4.66e-13	3.0	1.59e-09	2.0
14	5.82e-14	3.0	**5.82e-14**	3.0	5.82e-14	3.0	5.82e-14	3.0	3.97e-10	2.0

TABLE 2
Reconstruction results for $u_s(x)$ at $x = 0$ with $p = 2$.

n	$h^{0.5}$		h^1		h^2		h^3		h^4	
	Error	c.r.	Error	c.r.	Error	c.r.	Error	c.r.	Error	c.r.
1	3.25e-02	–	2.87e-02	–	1.10e-02	–	1.06e-02	–	2.21e-02	–
2	4.05e-03	3.0	4.17e-03	2.8	4.53e-03	1.3	2.10e-03	2.3	4.57e-03	2.3
3	4.98e-04	3.0	5.01e-04	3.1	5.37e-04	3.1	**6.04e-04**	1.8	**9.28e-04**	2.3
4	6.23e-05	3.0	6.24e-05	3.0	6.42e-05	3.1	**8.78e-05**	2.8	**2.00e-04**	2.2
5	7.80e-06	3.0	7.80e-06	3.0	**7.90e-06**	3.0	**1.12e-05**	3.0	***4.60e-05***	2.1
6	9.76e-07	3.0	9.76e-07	3.0	**9.82e-07**	3.0	**1.41e-06**	3.0	***1.10e-05***	2.1
7	1.22e-07	3.0	1.22e-07	3.0	**1.22e-07**	3.0	***1.75e-07***	3.0	***2.69e-06***	2.0
8	1.53e-08	3.0	1.53e-08	3.0	**1.53e-08**	3.0	***2.19e-08***	3.0	***6.66e-07***	2.0
9	1.91e-09	3.0	1.91e-09	3.0	**1.91e-09**	3.0	***2.73e-09***	3.0	***1.66e-07***	2.0
10	2.38e-10	3.0	**2.38e-10**	3.0	***2.38e-10***	3.0	***3.41e-10***	3.0	***4.13e-08***	2.0
11	2.98e-11	3.0	**2.98e-11**	3.0	***2.98e-11***	3.0	***4.26e-11***	3.0	***1.03e-08***	2.0
12	3.73e-12	3.0	**3.73e-12**	3.0	***3.73e-12***	3.0	***5.33e-12***	3.0	***2.58e-09***	2.0
13	4.66e-13	3.0	**4.66e-13**	3.0	***4.66e-13***	3.0	***6.66e-13***	3.0	***6.44e-10***	2.0
14	5.82e-14	3.0	**5.82e-14**	3.0	***5.82e-14***	3.0	***8.33e-14***	3.0	***1.61e-10***	2.0

TABLE 3
Reconstruction results for $u_s(x)$ at $x = 0$ with $p = 1$.

n	h^1		h^2		h^3		h^4	
	Error	c.r.	Error	c.r.	Error	c.r.	Error	c.r.
1	3.25e-02	–	2.65e-02	–	1.32e-02	–	2.46e-03	–
2	4.06e-03	3.0	4.32e-03	2.6	3.84e-03	1.8	1.98e-04	3.6
3	4.99e-04	3.0	5.17e-04	3.1	**5.92e-04**	2.7	**5.21e-05**	1.9
4	6.23e-05	3.0	6.33e-05	3.0	**7.67e-05**	2.9	**2.21e-05**	1.2
5	7.80e-06	3.0	**7.85e-06**	3.0	**9.59e-06**	3.0	***7.46e-06***	1.6
6	9.76e-07	3.0	**9.79e-07**	3.0	**1.19e-06**	3.0	***2.17e-06***	1.8
7	1.22e-07	3.0	**1.22e-07**	3.0	***1.49e-07***	3.0	***5.83e-07***	1.9
8	1.53e-08	3.0	**1.53e-08**	3.0	***1.86e-08***	3.0	***1.51e-07***	1.9
9	1.91e-09	3.0	**1.91e-09**	3.0	***2.32e-09***	3.0	***3.85e-08***	2.0
10	**2.38e-10**	3.0	***2.38e-10***	3.0	***2.90e-10***	3.0	***9.72e-09***	2.0
11	**2.98e-11**	3.0	***2.98e-11***	3.0	***3.62e-11***	3.0	***2.44e-09***	2.0
12	**3.73e-12**	3.0	***3.73e-12***	3.0	***4.53e-12***	3.0	***6.11e-10***	2.0
13	**4.66e-13**	3.0	***4.66e-13***	3.0	***5.66e-13***	3.0	***1.53e-10***	2.0
14	**5.82e-14**	3.0	***5.82e-14***	3.0	***7.08e-14***	3.0	***3.83e-11***	2.0

TABLE 4
Reconstruction results for $u_s(x)$ at $x = 0$ with $p = 4$.

n	$h^{0.25}$		$h^{0.5}$		h^3		h^4	
	Error	c.r.	Error	c.r.	Error	c.r.	Error	c.r.
1	2.85e-02	–	2.44e-02	–	2.48e-02	–	2.63e-02	–
2	4.09e-03	2.8	4.16e-03	2.6	2.13e-03	3.5	6.50e-03	2.0
3	4.98e-04	3.0	4.99e-04	3.1	**4.05e-04**	2.4	**1.56e-03**	2.1
4	6.23e-05	3.0	6.23e-05	3.0	**9.86e-05**	2.0	**3.73e-04**	2.1
5	7.80e-06	3.0	7.80e-06	3.0	**1.40e-05**	2.8	***8.99e-05***	2.1
6	9.76e-07	3.0	9.76e-07	3.0	**1.80e-06**	3.0	***2.20e-05***	2.0
7	1.22e-07	3.0	1.22e-07	3.0	***2.27e-07***	3.0	***5.43e-06***	2.0
8	1.53e-08	3.0	1.53e-08	3.0	***2.84e-08***	3.0	***1.35e-06***	2.0
9	1.91e-09	3.0	1.91e-09	3.0	***3.55e-09***	3.0	***3.36e-07***	2.0
10	2.38e-10	3.0	2.38e-10	3.0	***4.44e-10***	3.0	***8.39e-08***	2.0
11	2.98e-11	3.0	2.98e-11	3.0	***5.55e-11***	3.0	***2.09e-08***	2.0
12	3.73e-12	3.0	3.73e-12	3.0	***6.93e-12***	3.0	***5.23e-09***	2.0
13	4.66e-13	3.0	4.66e-13	3.0	***8.67e-13***	3.0	***1.31e-09***	2.0
14	5.82e-14	3.0	5.82e-14	3.0	***1.08e-13***	3.0	***3.27e-10***	2.0

TABLE 5
Reconstruction results for $u_d(x)$ at $x = 0$ with $p = 2$.

n	10^{20}		h^1		10^{-3}		10^{-6}		10^{-100}	
	Error	c.r.	Error	c.r.	Error	c.r.	Error	c.r.	Error	c.r.
1	3.64e-01	–	2.01e-01	–	1.54e-01	–	1.54e-01	–	1.54e-01	–
2	3.37e-01	0.1	3.99e-02	2.3	2.52e-02	2.6	2.52e-02	2.6	2.52e-02	2.6
3	3.34e-01	0.0	9.26e-03	2.1	4.82e-03	2.4	4.82e-03	2.4	4.82e-03	2.4
4	3.33e-01	0.0	2.25e-03	2.0	1.02e-03	2.2	1.02e-03	2.2	1.02e-03	2.2
5	3.33e-01	0.0	5.53e-04	2.0	2.32e-04	2.1	2.32e-04	2.1	2.32e-04	2.1
6	3.33e-01	0.0	1.37e-04	2.0	5.55e-05	2.1	5.50e-05	2.1	5.50e-05	2.1
7	3.33e-01	0.0	3.42e-05	2.0	1.39e-05	2.0	1.34e-05	2.0	1.34e-05	2.0
8	3.33e-01	0.0	8.54e-06	2.0	3.84e-06	1.9	3.30e-06	2.0	3.30e-06	2.0
9	3.33e-01	0.0	2.13e-06	2.0	1.36e-06	1.5	8.20e-07	2.0	8.20e-07	2.0
10	3.33e-01	0.0	**5.33e-07**	2.0	7.43e-07	0.9	2.04e-07	2.0	2.04e-07	2.0
11	3.33e-01	0.0	**1.33e-07**	2.0	5.90e-07	0.3	5.10e-08	2.0	5.10e-08	2.0
12	3.33e-01	0.0	**3.33e-08**	2.0	5.51e-07	0.1	1.27e-08	2.0	1.27e-08	2.0
13	3.33e-01	0.0	**8.33e-09**	2.0	5.42e-07	0.0	3.18e-09	2.0	3.18e-09	2.0
14	3.33e-01	0.0	**2.08e-09**	2.0	5.39e-07	0.0	7.95e-10	2.0	7.95e-10	2.0

TABLE 6
Reconstruction results for $u_d(x)$ at $x = 0$ with $p = 2$.

n	$h^{0.5}$		h^1		h^2		h^3		h^4	
	Error	c.r.	Error	c.r.	Error	c.r.	Error	c.r.	Error	c.r.
1	2.25e-01	–	2.01e-01	–	1.72e-01	–	1.61e-01	–	1.57e-01	–
2	7.25e-02	1.6	3.99e-02	2.3	2.61e-02	2.7	2.52e-02	2.7	2.52e-02	2.6
3	3.49e-02	1.1	9.26e-03	2.1	4.88e-03	2.4	**4.82e-03**	2.4	**4.82e-03**	2.4
4	1.88e-02	0.9	2.25e-03	2.0	1.02e-03	2.3	**1.02e-03**	2.2	**1.02e-03**	2.2
5	1.03e-02	0.9	5.53e-04	2.0	**2.32e-04**	2.1	**2.32e-04**	2.1	***2.32e-04***	2.1
6	5.52e-03	0.9	1.37e-04	2.0	**5.50e-05**	2.1	**5.50e-05**	2.1	***5.50e-05***	2.1
7	2.92e-03	0.9	3.42e-05	2.0	**1.34e-05**	2.0	***1.34e-05***	2.0	***1.34e-05***	2.0
8	1.52e-03	0.9	8.54e-06	2.0	**3.30e-06**	2.0	***3.30e-06***	2.0	***3.30e-06***	2.0
9	7.83e-04	1.0	2.13e-06	2.0	**8.20e-07**	2.0	***8.20e-07***	2.0	***8.20e-07***	2.0
10	4.00e-04	1.0	**5.33e-07**	2.0	***2.04e-07***	2.0	***2.04e-07***	2.0	***2.04e-07***	2.0
11	2.03e-04	1.0	**1.33e-07**	2.0	***5.10e-08***	2.0	***5.10e-08***	2.0	***5.10e-08***	2.0
12	1.03e-04	1.0	**3.33e-08**	2.0	***1.27e-08***	2.0	***1.27e-08***	2.0	***1.27e-08***	2.0
13	5.17e-05	1.0	**8.33e-09**	2.0	***3.18e-09***	2.0	***3.18e-09***	2.0	***3.18e-09***	2.0
14	2.60e-05	1.0	**2.08e-09**	2.0	***7.95e-10***	2.0	***7.95e-10***	2.0	***7.95e-10***	2.0

could be seen as an advantage when considering error estimation and adaptive grid refinement. Thus, at least from this example, for $p = 2$ the choice $q = 1$ within the range $[1, 3]$ (which also guarantees second order if at least one of the involved stencils is within a smooth region) seems to be preferable, and accordingly $q = 2$ for $p = 1$ and $q = 0.5$ for $p = 4$.

Tables 5, 6, 7 and 8 show the reconstruction errors $|P(0) - u_d(0)|$ and the resulting convergence rates for the nonsmooth example. Here, the choice $\varepsilon(h) = 10^{20}$ and therewith $P \approx P_{\text{opt}}$ does not yield convergence. The whole (non)smoothness information contained in the smoothness indicators gets lost against $\varepsilon(h)$. Similarly (see Remark 3.3), the error stagnates for $\varepsilon(h) = 10^{-3}$ in the considered range for the mesh size h. Even though this might not be of practical relevance, the same effect can be expected for $\varepsilon(h) = 10^{-6}$ (and even $\varepsilon(h) = 10^{-100}$) after further refinement steps, whereas second order accuracy can be observed so far. For the variable choice $\varepsilon(h) = h^q$ with $q \geq 2/p$, second order accuracy can be observed in all cases, whereas $q < 2/p$ leads to an order reduction (see again Remark 3.3).

TABLE 7
Reconstruction results for $u_d(x)$ at $x = 0$ with $p = 1$.

n	h^1		h^2		h^3		h^4	
	Error	c.r.	Error	c.r.	Error	c.r.	Error	c.r.
1	2.76e-01	–	2.45e-01	–	2.25e-01	–	2.15e-01	–
2	1.17e-01	1.2	5.18e-02	2.2	3.32e-02	2.8	2.91e-02	2.9
3	6.03e-02	1.0	1.16e-02	2.2	**5.62e-03**	2.6	**5.01e-03**	2.5
4	3.17e-02	0.9	2.72e-03	2.1	**1.11e-03**	2.3	**1.03e-03**	2.3
5	1.64e-02	1.0	**6.57e-04**	2.0	**2.43e-04**	2.2	***2.32e-04***	2.1
6	8.35e-03	1.0	**1.62e-04**	2.0	**5.64e-05**	2.1	***5.50e-05***	2.1
7	4.22e-03	1.0	**4.00e-05**	2.0	***1.36e-05***	2.1	***1.34e-05***	2.0
8	2.12e-03	1.0	**9.96e-06**	2.0	***3.32e-06***	2.0	***3.30e-06***	2.0
9	1.06e-03	1.0	**2.48e-06**	2.0	***8.22e-07***	2.0	***8.20e-07***	2.0
10	**5.32e-04**	1.0	***6.20e-07***	2.0	***2.04e-07***	2.0	***2.04e-07***	2.0
11	**2.66e-04**	1.0	***1.55e-07***	2.0	***5.10e-08***	2.0	***5.10e-08***	2.0
12	**1.33e-04**	1.0	***3.87e-08***	2.0	1.27e-08	2.0	***1.27e-08***	2.0
13	**6.66e-05**	1.0	***9.68e-09***	2.0	3.18e-09	2.0	***3.18e-09***	2.0
14	**3.33e-05**	1.0	***2.42e-09***	2.0	7.95e-10	2.0	***7.95e-10***	2.0

TABLE 8
Reconstruction results for $u_d(x)$ at $x = 0$ with $p = 4$.

n	$h^{0.25}$		$h^{0.5}$		h^3		h^4	
	Error	c.r.	Error	c.r.	Error	c.r.	Error	c.r.
1	1.70e-01	–	1.62e-01	–	1.47e-01	–	1.47e-01	–
2	3.73e-02	2.2	2.95e-02	2.5	2.51e-02	2.5	2.51e-02	2.5
3	1.31e-02	1.5	6.47e-03	2.2	**4.82e-03**	2.4	**4.82e-03**	2.4
4	6.32e-03	1.0	1.58e-03	2.0	**1.02e-03**	2.2	**1.02e-03**	2.2
5	3.52e-03	0.8	4.06e-04	2.0	**2.32e-04**	2.1	***2.32e-04***	2.1
6	2.04e-03	0.8	1.06e-04	1.9	**5.50e-05**	2.1	***5.50e-05***	2.1
7	1.18e-03	0.8	2.79e-05	1.9	***1.34e-05***	2.0	***1.34e-05***	2.0
8	6.76e-04	0.8	7.25e-06	1.9	***3.30e-06***	2.0	***3.30e-06***	2.0
9	3.81e-04	0.8	1.87e-06	2.0	***8.20e-07***	2.0	***8.20e-07***	2.0
10	2.12e-04	0.8	4.79e-07	2.0	***2.04e-07***	2.0	***2.04e-07***	2.0
11	1.16e-04	0.9	1.22e-07	2.0	***5.10e-08***	2.0	***5.10e-08***	2.0
12	6.28e-05	0.9	3.08e-08	2.0	***1.27e-08***	2.0	***1.27e-08***	2.0
13	3.36e-05	0.9	7.78e-09	2.0	***3.18e-09***	2.0	***3.18e-09***	2.0
14	1.78e-05	0.9	1.96e-09	2.0	***7.95e-10***	2.0	***7.95e-10***	2.0

4.2. The full scheme: Linear equation. In this example we consider the fully discrete scheme from section 2.3 applied to the linear transport equation

$$u_t + u_x = 0$$

with initial conditions (from [12])

$$u_0(x) = \sin\left(\pi x - \sin(\pi x)/\pi\right)$$

on the computational domain $x \in [-1, 1]$ (with periodic boundary conditions) and final time $T = 2$. We vary the number of grid points $Nx = 40 \cdot 2^n$ with $n \in \{0, \ldots, 7\}$, corresponding to $h = 0.05 \cdot 2^{-n}$, and restrict ourselves to the most promising candidates $\varepsilon(h) \in \{h^1, h^2, h^3, 10^{-3}, 10^{-6}\}$ for the usual choice $p = 2$, and we further consider $p = 1$ and $p = 4$ for the same choice of $\varepsilon(h)$. The time step size is chosen to be $\Delta t \approx 0.9\frac{h}{f'_{\max}}$ with $f'_{\max} = 1$.

Tables 9 to 14 show the errors of the computed numerical solutions compared to the analytical solution in the L^1 and the L^∞ norm, and the resulting convergence rates. Most of the impressions received from the numerical results in the smooth

TABLE 9
L^1 error in the linear accuracy test for $p = 2$.

Nx	h^1		h^2		h^3		10^{-3}		10^{-6}	
	Error	c.r.	Error	c.r.	Error	c.r.	Error	c.r.	Error	c.r.
40	1.02e-02	–	3.29e-02	–	**9.35e-02**	–	5.02e-02	–	1.03e-01	–
80	1.17e-03	3.1	**4.66e-03**	2.8	**2.42e-02**	2.0	3.64e-03	3.8	3.04e-02	1.8
160	1.42e-04	3.0	**5.60e-04**	3.1	**3.98e-03**	2.6	2.16e-04	4.1	5.38e-03	2.5
320	1.76e-05	3.0	**6.62e-05**	3.1	***6.70e-04***	2.6	1.87e-05	3.5	4.18e-04	3.7
640	2.19e-06	3.0	**8.10e-06**	3.0	***1.22e-04***	2.5	2.22e-06	3.1	2.76e-05	3.9
1280	2.73e-07	3.0	**1.01e-06**	3.0	***2.24e-05***	2.4	2.73e-07	3.0	1.59e-06	4.1
2560	**3.41e-08**	3.0	***1.26e-07***	3.0	***4.12e-06***	2.4	3.40e-08	3.0	9.82e-08	4.0
5120	**4.25e-09**	3.0	***1.57e-08***	3.0	***7.57e-07***	2.4	4.25e-09	3.0	6.42e-09	3.9

TABLE 10
L^∞ error in the linear accuracy test for $p = 2$.

Nx	h^1		h^2		h^3		10^{-3}		10^{-6}	
	Error	c.r.	Error	c.r.	Error	c.r.	Error	c.r.	Error	c.r.
40	1.45e-02	–	4.93e-02	–	**1.19e-01**	–	7.29e-02	–	1.29e-01	–
80	1.69e-03	3.1	**1.03e-02**	2.3	**4.29e-02**	1.5	7.92e-03	3.2	5.11e-02	1.3
160	1.92e-04	3.1	**1.67e-03**	2.6	**1.27e-02**	1.8	4.63e-04	4.1	1.56e-02	1.7
320	2.30e-05	3.1	**2.30e-04**	2.9	***3.66e-03***	1.8	3.02e-05	3.9	2.37e-03	2.7
640	2.83e-06	3.0	**2.93e-05**	3.0	***1.13e-03***	1.7	2.95e-06	3.4	2.06e-04	3.5
1280	3.52e-07	3.0	**3.65e-06**	3.0	***3.51e-04***	1.7	3.53e-07	3.1	8.23e-06	4.6
2560	**4.39e-08**	3.0	***4.54e-07***	3.0	***1.08e-04***	1.7	4.39e-08	3.0	2.97e-07	4.8
5120	**5.48e-09**	3.0	***5.66e-08***	3.0	***3.34e-05***	1.7	5.48e-09	3.0	1.36e-08	4.4

TABLE 11
L^1 error in the linear accuracy test for $p = 1$.

Nx	h^1		h^2		h^3		10^{-3}		10^{-6}	
	Error	c.r.	Error	c.r.	Error	c.r.	Error	c.r.	Error	c.r.
40	9.29e-03	–	1.70e-02	–	**4.01e-02**	–	2.27e-02	–	6.57e-02	–
80	1.14e-03	3.0	**2.25e-03**	2.9	**7.87e-03**	2.3	1.86e-03	3.6	1.33e-02	2.3
160	1.41e-04	3.0	**2.68e-04**	3.1	**1.50e-03**	2.4	1.59e-04	3.6	1.75e-03	2.9
320	1.75e-05	3.0	**3.20e-05**	3.1	***2.86e-04***	2.4	1.80e-05	3.1	1.88e-04	3.2
640	2.18e-06	3.0	**3.94e-06**	3.0	***5.42e-05***	2.4	2.20e-06	3.0	1.30e-05	3.9
1280	2.72e-07	3.0	**4.91e-07**	3.0	***1.02e-05***	2.4	2.73e-07	3.0	7.58e-07	4.1
2560	**3.40e-08**	3.0	***6.13e-08***	3.0	***1.91e-06***	2.4	3.40e-08	3.0	5.04e-08	3.9
5120	**4.25e-09**	3.0	***7.66e-09***	3.0	***3.56e-07***	2.4	4.25e-09	3.0	4.81e-09	3.4

TABLE 12
L^∞ error in the linear accuracy test for $p = 1$.

Nx	h^1		h^2		h^3		10^{-3}		10^{-6}	
	Error	c.r.	Error	c.r.	Error	c.r.	Error	c.r.	Error	c.r.
40	1.18e-02	–	2.90e-02	–	**6.31e-02**	–	3.89e-02	–	9.03e-02	–
80	1.49e-03	3.0	**5.50e-03**	2.4	**2.00e-02**	1.7	4.30e-03	3.2	3.03e-02	1.6
160	1.83e-04	3.0	**8.66e-04**	2.7	**6.26e-03**	1.7	2.87e-04	3.9	7.21e-03	2.1
320	2.26e-05	3.0	**1.19e-04**	2.9	***1.95e-03***	1.7	2.47e-05	3.5	1.24e-03	2.5
640	2.82e-06	3.0	**1.52e-05**	3.0	***6.06e-04***	1.7	2.85e-06	3.1	1.04e-04	3.6
1280	3.51e-07	3.0	**1.89e-06**	3.0	***1.88e-04***	1.7	3.52e-07	3.0	4.18e-06	4.6
2560	**4.39e-08**	3.0	***2.36e-07***	3.0	***5.79e-05***	1.7	4.39e-08	3.0	1.59e-07	4.7
5120	**5.48e-09**	3.0	***2.94e-08***	3.0	***1.77e-05***	1.7	5.48e-09	3.0	8.56e-09	4.2

TABLE 13
L^1 error in the linear accuracy test for $p = 4$.

Nx	h^1		h^2		h^3		10^{-3}		10^{-6}	
	Error	c.r.	Error	c.r.	Error	c.r.	Error	c.r.	Error	c.r.
40	1.30e-02	–	8.15e-02	–	**1.17e-01**	–	1.01e-01	–	1.20e-01	–
80	1.29e-03	3.3	**1.00e-02**	3.0	**4.07e-02**	1.5	7.71e-03	3.7	4.20e-02	1.5
160	1.46e-04	3.1	**1.20e-03**	3.1	**1.08e-02**	1.9	3.93e-04	4.3	1.10e-02	1.9
320	1.78e-05	3.0	**1.37e-04**	3.1	***2.62e-03***	2.0	2.31e-05	4.1	1.11e-03	3.3
640	2.20e-06	3.0	**1.66e-05**	3.0	***3.79e-04***	2.8	2.26e-06	3.4	5.85e-05	4.2
1280	2.74e-07	3.0	**2.06e-06**	3.0	***5.10e-05***	2.9	2.75e-07	3.0	3.27e-06	4.2
2560	**3.41e-08**	3.0	***2.57e-07***	3.0	***8.87e-06***	2.5	3.41e-08	3.0	1.98e-07	4.0
5120	**4.26e-09**	3.0	***3.21e-08***	3.0	***1.62e-06***	2.5	4.25e-09	3.0	1.15e-08	4.1

TABLE 14
L^∞ error in the linear accuracy test for $p = 4$.

Nx	h^1		h^2		h^3		10^{-3}		10^{-6}	
	Error	c.r.	Error	c.r.	Error	c.r.	Error	c.r.	Error	c.r.
40	2.05e-02	–	1.13e-01	–	**1.38e-01**	–	1.28e-01	–	1.40e-01	–
80	2.18e-03	3.2	**1.90e-02**	2.6	**6.28e-02**	1.1	1.48e-02	3.1	6.79e-02	1.0
160	2.21e-04	3.3	**3.26e-03**	2.5	**2.51e-02**	1.3	8.28e-04	4.2	2.56e-02	1.4
320	2.43e-05	3.2	**4.54e-04**	2.8	***9.73e-03***	1.4	4.27e-05	4.3	4.96e-03	2.4
640	2.89e-06	3.1	**5.77e-05**	3.0	***2.51e-03***	2.0	3.26e-06	3.7	4.05e-04	3.6
1280	3.54e-07	3.0	**7.17e-06**	3.0	***6.33e-04***	2.0	3.58e-07	3.2	1.64e-05	4.6
2560	**4.40e-08**	3.0	***8.90e-07***	3.0	***1.90e-04***	1.7	4.40e-08	3.0	5.76e-07	4.8
5120	**5.48e-09**	3.0	***1.11e-07***	3.0	***5.90e-05***	1.7	5.48e-09	3.0	2.40e-08	4.6

case in section 4.1 are confirmed. For $\varepsilon(h) = 10^{-3}$ third order accuracy is observed after a few refinement steps, and for $\varepsilon(h) = 10^{-6}$ the error in both norms is at least approaching the same size. For the variable parameter choice $\varepsilon(h) = h^q$, third order convergence can only be observed for $q = 1$ and $q = 2$ (for all considered choices of p), where $q = 1$ delivers the smaller absolute errors in both norms. Within further tests with different values for $q \in (2, 3]$, the observed convergence rates always significantly differed from three. Furthermore, we tried a different Riemann solver and also very small time step sizes Δt, and we made the same observation. Apparently, even though the (spatial) CTO-WENO reconstruction (at a fixed time) is third order accurate for $q \leq 3$, $q > 2$ does not lead to a third order scheme in total. The better convergence properties for $q \leq 2$ might be due to the fact that in this case $\varepsilon(h) = Kh^q$ is always part of the dominant term in the denominator in (3.10).

Concerning the different choices for the parameter p, one may observe that for $\varepsilon(h) = h^2$ the errors approximately linearly depend on p. This can be explained by the factor p in the leading error term in (3.13) (deviation from the optimal weight), which seems to be the dominant error term here.

4.3. The full scheme: Nonlinear equation. As a third example we consider the nonlinear Burgers equation

$$u_t + \left(\tfrac{1}{2}u^2\right)_x = 0$$

with initial conditions

$$u_0(x) = 1 + \tfrac{1}{2}\sin(\pi x)$$

on the computational domain $x \in [-1, 1]$ (with periodic boundary conditions). For the given initial conditions, a discontinuity evolves at time $T_d = 2/\pi$. As in [16],

TABLE 15
L^1 error for the nonlinear test case at $T = 0.33$.

Nx	h^1		h^2		h^3		10^{-3}		10^{-6}	
	Error	c.r.	Error	c.r.	Error	c.r.	Error	c.r.	Error	c.r.
40	8.45e-04	–	1.88e-03	–	**7.30e-03**	–	2.80e-03	–	9.88e-03	–
80	1.08e-04	3.0	**2.04e-04**	3.2	**1.18e-03**	2.6	1.72e-04	4.0	2.42e-03	2.0
160	1.37e-05	3.0	**2.35e-05**	3.1	**1.80e-04**	2.7	1.51e-05	3.5	2.45e-04	3.3
320	1.72e-06	3.0	**2.86e-06**	3.0	***2.99e-05***	2.6	1.74e-06	3.1	1.39e-05	4.1
640	2.16e-07	3.0	**3.53e-07**	3.0	***5.05e-06***	2.6	2.16e-07	3.0	7.96e-07	4.1
1280	2.71e-08	3.0	**4.40e-08**	3.0	***8.59e-07***	2.6	2.71e-08	3.0	5.84e-08	3.8
2560	**3.39e-09**	3.0	***5.48e-09***	3.0	***1.47e-07***	2.5	3.39e-09	3.0	4.77e-09	3.6
5120	**4.23e-10**	3.0	***6.84e-10***	3.0	***2.55e-08***	2.5	4.23e-10	3.0	4.56e-10	3.4

TABLE 16
L^∞ error for the nonlinear test case at $T = 0.33$.

Nx	h^1		h^2		h^3		10^{-3}		10^{-6}	
	Error	c.r.	Error	c.r.	Error	c.r.	Error	c.r.	Error	c.r.
40	4.02e-03	–	8.15e-03	–	**3.75e-02**	–	1.04e-02	–	4.98e-02	–
80	6.06e-04	2.7	**7.87e-04**	3.4	**4.88e-03**	2.9	7.00e-04	3.9	1.37e-02	1.9
160	8.32e-05	2.9	**8.55e-05**	3.2	**1.19e-03**	2.0	7.40e-05	3.2	1.61e-03	3.1
320	1.08e-05	3.0	**1.02e-05**	3.1	***3.29e-04***	1.9	1.02e-05	2.9	1.29e-04	3.6
640	1.36e-06	3.0	**1.24e-06**	3.0	***9.05e-05***	1.9	1.34e-06	2.9	4.85e-06	4.7
1280	1.70e-07	3.0	**1.53e-07**	3.0	***2.48e-05***	1.9	1.70e-07	3.0	1.84e-07	4.7
2560	**2.12e-08**	3.0	***1.88e-08***	3.0	***6.74e-06***	1.9	2.12e-08	3.0	1.81e-08	3.3
5120	**2.61e-09**	3.0	***2.29e-09***	3.0	***1.82e-06***	1.9	2.61e-09	3.0	2.22e-09	3.0

we consider the preshock accuracy at $T = 0.33$. Similar to section 4.2, we vary the number of grid points $Nx = 40 \cdot 2^n$ with $n \in \{0, \dots, 7\}$, corresponding to $h = 0.05 \cdot 2^{-n}$, and restrict ourselves to the candidates $\varepsilon(h) \in \{h^1, h^2, h^3, 10^{-3}, 10^{-6}\}$ and $p = 2$. The time step size is chosen to be $\Delta t \approx 0.9 \frac{h}{f'_{\max}}$ with $f'_{\max} = 1.5$.

Tables 15 and 16 show the errors of the computed numerical solutions compared to the analytical solution in the L^1 and the L^∞ norm, and the resulting convergence rates. The entire results are very similar to the linear test case in section 4.2. We observe third order convergence for $\varepsilon(h) \in \{10^{-3}, h^1, h^2\}$ almost from the beginning and an order reduction for $\varepsilon(h) = h^3$. For $\varepsilon(h) = 10^{-6}$ the initial errors are larger than for $\varepsilon(h) \in \{10^{-3}, h^1, h^2\}$, but it finally catches up after several refinements.

4.4. The full scheme: Nonlinear system. As a final example, we consider the one-dimensional Euler equations

$$\frac{\partial}{\partial t}\begin{pmatrix}\rho\\ m\\ E\end{pmatrix} + \frac{\partial}{\partial x}\begin{pmatrix}m\\ \rho v^2 + p\\ v(E+p)\end{pmatrix} = 0$$

with $p = (\gamma - 1)(E - \rho v^2/2)$, $\gamma = 1.4$, and $v = m/\rho$, and first, Sod's Riemann initial data from [21],

$$u(x,0) = \begin{cases}(1, 0, 2.5) & \text{for } x < 0.5,\\ (0.125, 0, 0.25) & \text{for } x > 0.5.\end{cases}$$

For the computations we use $Nx = 20 \cdot 2^n$ grid points in $[0, 1]$ ($n \in \{0, \dots, 7\}$), $\Delta t \approx 0.9 \frac{h}{\lambda_{\max}}$ (with $\lambda_{\max} = 2.5$), and $T = 0.16$ as final time. Since $\varepsilon(h) = h^3$ did not deliver third order accuracy for the smooth test cases in sections 4.2 and 4.3, we

TABLE 17
L^1 error for the density ρ in Sod's problem at $T = 0.16$.

Nx	h^1		$h^{1.5}$		h^2		10^{-3}		10^{-6}	
	Error	c.r.	Error	c.r.	Error	c.r.	Error	c.r.	Error	c.r.
20	2.92e-02	–	2.98e-02	–	3.10e-02	–	3.14e-02	–	3.18e-02	–
40	1.88e-02	0.6	2.04e-02	0.6	**2.15e-02**	0.5	2.13e-02	0.6	2.20e-02	0.5
80	1.01e-02	0.9	1.09e-02	0.9	**1.11e-02**	1.0	1.09e-02	1.0	1.10e-02	1.0
160	5.48e-03	0.9	**5.81e-03**	0.9	**5.77e-03**	0.9	5.76e-03	0.9	5.64e-03	1.0
320	2.94e-03	0.9	**3.05e-03**	0.9	**3.03e-03**	0.9	3.01e-03	0.9	3.00e-03	0.9
640	1.58e-03	0.9	**1.61e-03**	0.9	**1.63e-03**	0.9	1.59e-03	0.9	1.63e-03	0.9
1280	**8.48e-04**	0.9	**8.71e-04**	0.9	***8.92e-04***	0.9	8.46e-04	0.9	8.91e-04	0.9
2560	**4.59e-04**	0.9	**4.81e-04**	0.9	***4.94e-04***	0.9	4.56e-04	0.9	4.91e-04	0.9

leave out this choice here and further consider $\varepsilon(h) = h^{1.5}$ instead for possibly more insight between the choices $q = 1$ and $q = 2$.

Table 17 shows the L^1 error for the computed densities ρ at the final time compared to the analytical solution. The absolute errors are almost identical for all choices of $\varepsilon(h)$; only slight advantages may be seen for $\varepsilon(h) = h^1$ and $\varepsilon(h) = 10^{-3}$ – thus for the "largest" choices of $\varepsilon(h)$. On the other hand, when taking a closer look at the plots of the corresponding solutions (see Figure 1 for the comparison of $\varepsilon(h) = h^1$

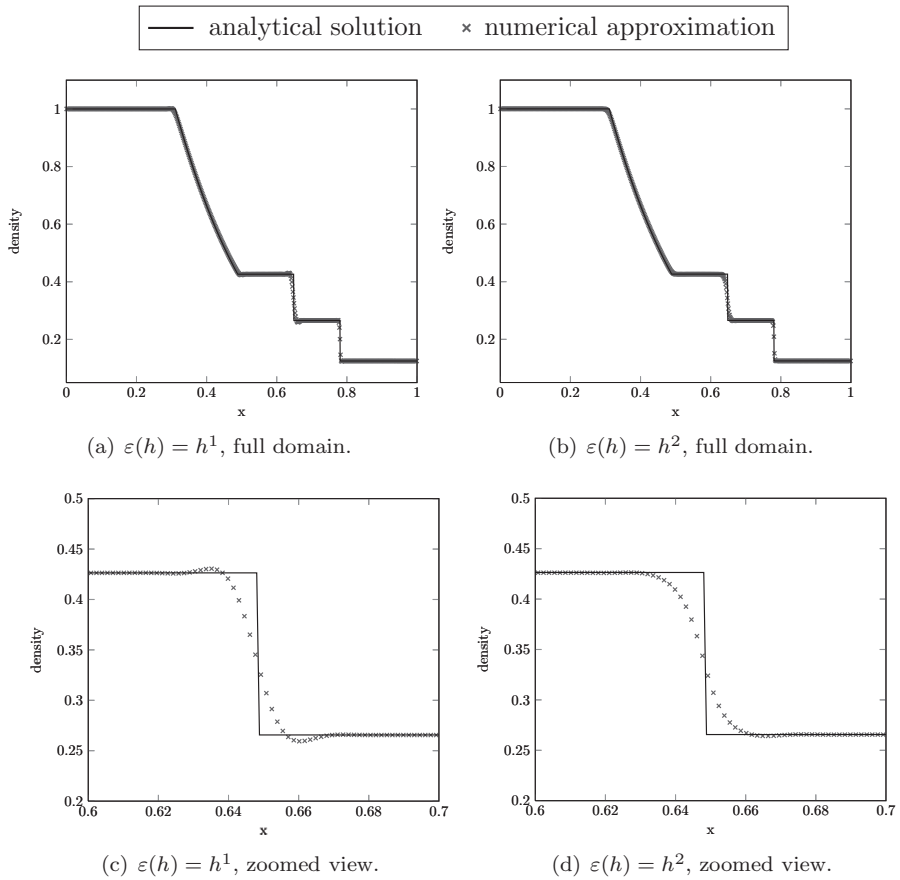

(a) $\varepsilon(h) = h^1$, full domain. (b) $\varepsilon(h) = h^2$, full domain.

(c) $\varepsilon(h) = h^1$, zoomed view. (d) $\varepsilon(h) = h^2$, zoomed view.

FIG. 1. *Results for Sod's problem with $Nx = 640$.*

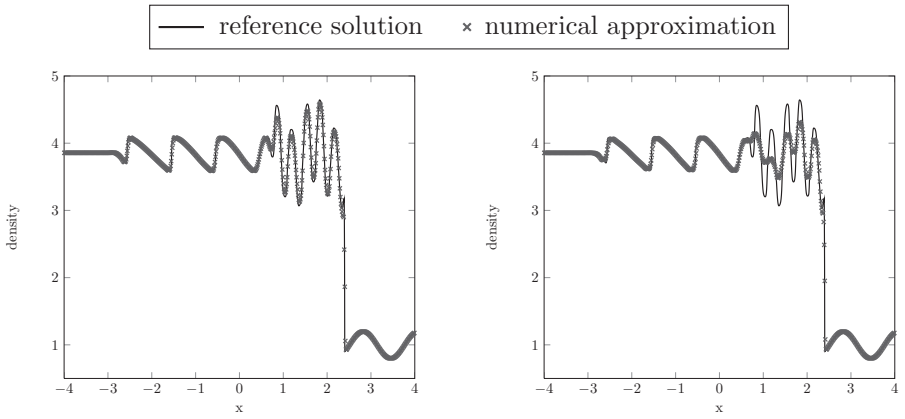

(a) $\varepsilon(h) = h^1$. (b) $\varepsilon(h) = h^2$.

FIG. 2. *Results for the shock-acoustic interaction problem with* $Nx = 640$.

and $\varepsilon(h) = h^2$), the over- and undershoots are smaller for $\varepsilon(h) \in \{h^{1.5}, h^2, 10^{-6}\}$. This effect does not change when we use locally defined characteristic variables in the CTO-WENO reconstruction (as proposed in [11]) instead of the conserved variables.

As a further test case for the Euler equations, we consider the shock-acoustic interaction example from [20], i.e., initial conditions

$$\begin{pmatrix}\rho\\ v\\ p\end{pmatrix}(x,0) = \begin{cases}(3.857143,\ 2.629369,\ 10.33333) & \text{for } x < -4,\\ (1+\delta\sin(5x),\ 0,\ 1) & \text{for } x \geq 4\end{cases}$$

with $\delta = 0.2$. The analytical solution for this example consists of a moving shock wave interacting with sine waves in the density. Thus for the numerical solution, high order resolution for the resulting fine (smooth) structures in the density profile is desirable as well as a stable treatment of the shock at the same time here.

Figure 2 shows the computed densities ρ at the final time $T = 1.8$ for $Nx = 640$ grid points in $[-4, 4]$ and $\varepsilon(h) \in \{h^1, h^2\}$. The reference solution has been computed with $Nx = 2560$ grid points. Both choices of $\varepsilon(h)$ resolve the shock with the same accuracy, but $\varepsilon(h) = h^1$ obviously performs much better for the fine structures in the density profile behind the shock.

5. Conclusion. We considered the convergence properties of a compact third order WENO reconstruction procedure. Even though the results of [1] cannot be applied to this scheme, we could show comparable convergence results, even allowing for a wider parameter range. In particular, for $p = 2$ the choice $\varepsilon(h) = h^q$ with $q = 1$ at the lower "admissible" bound convinces with a fast conformance of the observed convergence rates with the predicted ones, which might be beneficial when applied for error estimation or within adaptive schemes. The choice $q = 3$ at the upper bound showed the optimal convergence rates for pure reconstructions but a lower convergence rate within the fully discrete scheme; at least it could not be observed within the applied range for the mesh size h. On the other hand, in the vicinity of discontinuities, smaller values for $\varepsilon(h)$ and thus higher values for q yield smaller oscillations. Therefore, for $p = 2$, the "optimal" value for q might lie somewhere between 1 and 2. Alternatively, one could think of a piecewise definition of $\varepsilon(h)$,

for instance, $\varepsilon(h) = \min\{10^{-3}, h^2\}$, to quickly achieve the desired accuracy but also assert vanishing oscillations for $h \to 0$.

REFERENCES

[1] F. Aràndiga, A. Baeza, A. M. Belda, and P. Mulet, *Analysis of WENO schemes for full and global accuracy*, SIAM J. Numer. Anal., 49 (2011), pp. 893–915.

[2] D. S. Balsara and C.-W. Shu, *Monotonicity preserving weighted essentially non-oscillatory schemes with increasingly high order of accuracy*, J. Comput. Phys., 160 (2000), pp. 405–452.

[3] R. Borges, M. Carmona, B. Costa, and W. S. Don, *An improved weighted essentially non-oscillatory scheme for hyperbolic conservation laws*, J. Comput. Phys., 227 (2008), pp. 3191–3211.

[4] S. Bryson and D. Levy, *Mapped WENO and weighted power ENO reconstructions in semi-discrete central schemes for Hamilton-Jacobi equations*, Appl. Numer. Math., 56 (2006), pp. 1211–1224.

[5] M. Castro, B. Costa, and W. S. Don, *High order weighted essentially non-oscillatory WENO-Z schemes for hyperbolic conservation laws*, J. Comput. Phys., 230 (2011), pp. 1766–1792.

[6] W.-S. Don and R. Borges, *Accuracy of the weighted essentially non-oscillatory conservative finite difference schemes*, J. Comput. Phys., 250 (2013), pp. 347–372.

[7] H. Feng, F. Hu, and R. Wang, *A new mapped weighted essentially non-oscillatory scheme*, J. Sci. Comput., 51 (2012), pp. 449–473.

[8] G. A. Gerolymos, D. Sénéchal, and I. Vallet, *Very-high-order WENO schemes*, J. Comput. Phys., 228 (2009), pp. 8481–8524.

[9] S. Gottlieb and C.-W. Shu, *Total variation diminishing Runge-Kutta schemes*, Math. Comp., 67 (1998), pp. 73–85.

[10] Y. Ha, C. Ho Kim, Y. Ju Lee, and J. Yoon, *An improved weighted essentially non-oscillatory scheme with a new smoothness indicator*, J. Comput. Phys., 232 (2013), pp. 68–86.

[11] A. Harten, B. Engquist, S. Osher, and S. R. Chakravarthy, *Uniformly high order accurate essentially non-oscillatory schemes,* III, J. Comput. Phys., 71 (1987), pp. 231–303.

[12] A. K. Henrick, T. D. Aslam, and J. M. Powers, *Mapped weighted essentially non-oscillatory schemes: Achieving optimal order near critical points*, J. Comput. Phys., 207 (2005), pp. 542–567.

[13] G.-S. Jiang and C.-W. Shu, *Efficient implementation of weighted ENO schemes*, J. Comput. Phys., 126 (1996), pp. 202–228.

[14] A. Kurganov and D. Levy, *A third-order semidiscrete central scheme for conservation laws and convection-diffusion equations*, SIAM J. Sci. Comput., 22 (2000), pp. 1461–1488.

[15] D. Levy, G. Puppo, and G. Russo, *Central WENO schemes for hyperbolic systems of conservation laws*, M2AN Math. Model. Numer. Anal., 33 (1999), pp. 547–571.

[16] D. Levy, G. Puppo, and G. Russo, *Compact central WENO schemes for multidimensional conservation laws*, SIAM J. Sci. Comput., 22 (2000), pp. 656–672.

[17] X.-D. Liu, S. Osher, and T. Chan, *Weighted essentially non-oscillatory schemes*, J. Comput. Phys., 115 (1994), pp. 200–212.

[18] S. Serna and A. Marquina, *Power ENO methods: A fifth-order accurate weighted power ENO method*, J. Comput. Phys., 194 (2004), pp. 632–658.

[19] C.-W. Shu, *High order weighted essentially nonoscillatory schemes for convection dominated problems*, SIAM Rev., 51 (2009), pp. 82–126.

[20] C.-W. Shu and S. Osher, *Efficient implementation of essentially non-oscillatory shock-capturing schemes,* II, J. Comput. Phys., 83 (1989), pp. 32–78.

[21] G. A. Sod, *A survey of several finite difference methods for systems of nonlinear hyperbolic conservation laws*, J. Comput. Phys., 27 (1978), pp. 1–31.

[22] N. K. Yamaleev and M. H. Carpenter, *A systematic methodology for constructing high-order energy stable WENO schemes*, J. Comput. Phys., 228 (2009), pp. 4248–4272.

[23] N. K. Yamaleev and M. H. Carpenter, *Third-order energy stable WENO scheme*, J. Comput. Phys., 228 (2009), pp. 3025–3047.